

# Functional Uncoupling of Linked Neurotransmitter Effects by Combinatorial Convergence

Vladimir Brezina,\* Irina V. Orekhova, Klaudiusz R. Weiss

Physiological signaling pathways both diverge and converge—a single neurotransmitter can have multiple effects and multiple transmitters can have the same effects—in the same target cell. Divergence couples the effects of a transmitter together in a relatively fixed ratio. Different physiological circumstances may require a different ratio, however; the coupling must be made modifiable. This can be achieved through convergence. If two transmitters couple the effects in different ratios, then combinations of the transmitters can yield all intermediate ratios of the effects, thus functionally uncoupling them. This mechanism is analyzed in a well-understood, simple invertebrate neuromuscular circuit.

In the nervous system and elsewhere, physiological signaling pathways characteristically branch or diverge because each upstream element tends to interact with multiple downstream elements. Thus, a single neurotransmitter typically acts through diverging cellular signaling pathways to affect multiple processes—for instance, activity of several ion channel types—in the same target cell (1, 2). Upon exposure to the transmitter, all of the effects appear together in a relatively fixed ratio of amplitudes and time courses. Divergence thus couples multiple effects into a single integrated response to a physiological stimulus. However, by itself it permits no flexibility when, under different physiological circumstances, a different coupling ratio or no coupling at all might be more advantageous. An additional mechanism is needed to uncouple the effects again, to different degrees, so that the effective coupling is not fixed, but variable. This uncoupling can best be achieved through modulation by a second transmitter. Modulation of this kind is usually thought of in terms of synergistic “cross-talk” or “gating” of specific pathway branches (3).

We suggest that a more elegant, general mechanism for functional uncoupling is in fact inherent in the basic structure of signaling pathways in many cells. It arises automatically from the fact that signaling pathways not only diverge but also converge. In particular, multiple transmitters often converge nonsynergistically on a common set of effects (1, 2). If two transmitters independently produce a common set of effects but the effects of each transmitter are coupled in a different ratio, then

combinations of the two transmitters give ratios of effects that neither transmitter can produce alone; in general, all intermediate ratios are possible. The coupled effects are

thus functionally uncoupled. In the extreme, the divergent and convergent linkages in the system may become effectively disconnected, so that each effect becomes independently controllable by just one transmitter, and each transmitter is tuned to produce just one effect. Beyond increasing physiological flexibility, such tuning has broader implications for specificity in signaling pathways. Alone, divergence and convergence both degrade specificity (2); when the two are combined, however, specificity may be preserved or even enhanced. Finally, we note that these phenomena depend only on the abstract, formal properties of divergence and convergence and might thus be expected in any signaling system with those properties.

We now demonstrate how this mechanism operates in a simple invertebrate neuromuscular circuit where we not only understand its cellular mechanisms but can suggest its likely behavioral significance. The accessory radula closer (ARC) muscle

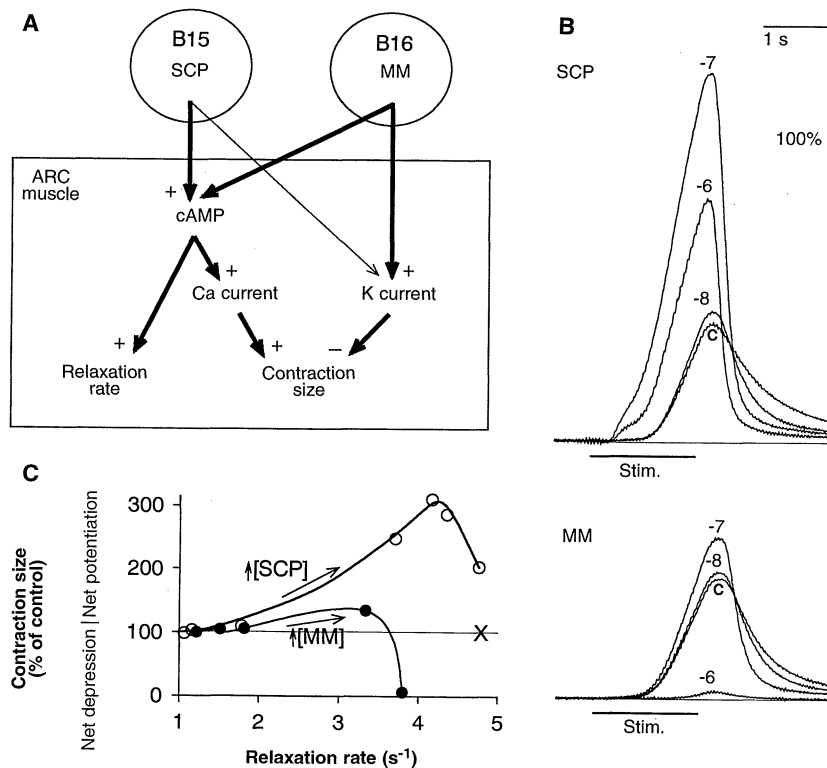


**Fig. 1.** (A) Signal divergence and convergence in the ARC muscle. (B) Typical SCP and MM effects on size and relaxation rate of ARC muscle contractions. These experiments were done as in (15). Briefly, motor neuron B16 spikes (not shown) were driven intracellularly with 14- to 24-ms depolarizing current pulses at 12 to 26 Hz for 1.5 s (“Stim”). Each of these spike bursts produced a contraction. Contractions were isotonic and essentially unloaded; length was monitored with an isotonic transducer. Contractions were induced every 30 s. With these stimulation parameters, no significant endogenous peptide release was expected (13, 14). Exogenous SCP<sub>B</sub> and MM<sub>A</sub> were applied to the muscle only (“c,” “-8,” “-7,” and “-6” indicate, respectively, control, 10<sup>-8</sup>, 10<sup>-7</sup>, and 10<sup>-6</sup> M); the contractions shown occurred after 5 min of exposure (10 contractions). All measurements were made after 5 min. (C) Plot of the contraction size and relaxation rate effects against each other [measurements from the records in (B) and additional concentrations]. Relaxation rate was measured as the reciprocal of the time taken by the contraction to decrease from peak amplitude to one-third of the peak amplitude (15).

Department of Physiology and Biophysics and the Fishberg Research Center in Neurobiology, Box 1218, Mount Sinai School of Medicine, 1 Gustave L. Levy Place, New York, NY 10029, USA.

\*To whom correspondence should be addressed.

of *Aplysia* participates in consummatory feeding behaviors such as biting and swallowing (4, 5). The muscle contracts in response to acetylcholine (ACh) released from either of its two motor neurons, B15 and B16 (4). These basal contractions are then shaped by numerous modulatory transmitters and peptides, released under appropriate behavioral circumstances from various sources, that converge on a common set of processes in the muscle (6–17). We focus here particularly on two peptide families, the small cardioactive peptides (SCPs) and the myomodulins (MMs), because these are released by the motor neurons themselves as cotransmitters: B15 releases the SCPs, and B16 the MMs (9–16). Thus, when B15 and B16 fire in different proportions, as they do in different behaviors (5), the effect is a variation of the SCP:MM ratio released onto the muscle.

Figure 1A shows how the signaling pathways diverge and converge in the ARC muscle. The ultimate functional result is modulation of two contraction parameters: size and relaxation rate (Fig. 1B). Relaxation rate is accelerated, whereas contraction size can be increased or decreased by competing potentiating and depressing mechanisms (15). Potentiation is caused by enhancement of Ca current in the muscle, resulting in increased Ca<sup>2+</sup> influx (15, 18), and depression by activation of K current, resulting in reduced ACh-induced depolarization, reduced activation of the Ca current, and reduced Ca<sup>2+</sup> influx (8, 15, 19). Asymmetry between the two mechanisms gives net potentiation at low modulator concentrations and increasing depression at higher concentrations (19) (Fig. 1, B and C). The relaxation rate effect, thought to affect the contractile machinery directly (20), and the Ca current enhancement are both mediated by adenosine 3',5',-monophosphate (cAMP) (9, 18, 21, 22). Thus, the acceleration of the relaxation rate and the potentiation of contraction size are tightly coupled. These processes are modulated identically by the SCPs and MMs. However, the SCPs and MMs differ in activating the K current. The MMs activate much larger K currents, and therefore have much stronger depressive effects, than the SCPs (Fig. 1, B and C) (23). By converging unequally on the K current but equally on cAMP (24), the SCPs and MMs produce different ratios of the ultimate effects on contraction size and relaxation rate (Fig. 1C). However, SCPs or MMs alone cannot give an arbitrary ratio; for example, a contraction unchanged in size but with greatly accelerated relaxation rate ("×" in Fig. 1C). A broad range of ratios can only be reached by release of the SCPs and MMs in combination.

Figure 2 shows experimental data and model relating modulation of Ca and K currents to contraction size. (A) Experimental data. Each point represents a measurement of contraction size after application of a particular modulator concentration, plotted against the extent to which that concentration modulates the Ca and K currents. (○) SCP<sub>A</sub> and SCP<sub>B</sub>; "A," MM<sub>A</sub>; "B," MM<sub>B</sub>; (●) MM<sub>C</sub> through MM<sub>I</sub>; (□) serotonin; and (■) FRF<sub>A</sub> through FRF<sub>C</sub>. For details, see (29, 30). (B) Model. The relation between the Ca and K current values Ca and K and the contraction size S is assumed to have the form

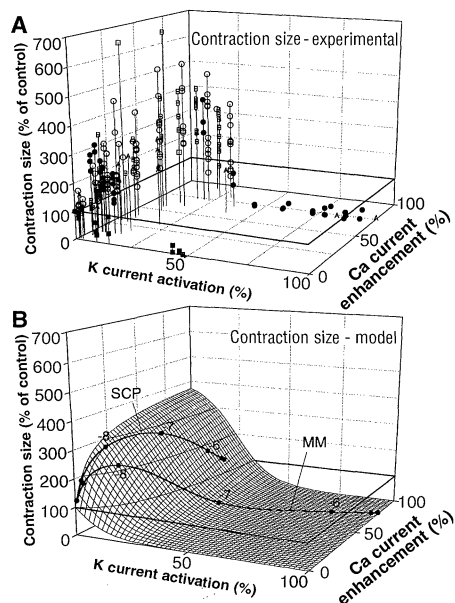


**Fig. 2.** Experimental data and model relating modulation of Ca and K currents to contraction size. (A) Experimental data. Each point represents a measurement of contraction size after application of a particular modulator concentration, plotted against the extent to which that concentration modulates the Ca and K currents. (○) SCP<sub>A</sub> and SCP<sub>B</sub>; "A," MM<sub>A</sub>; "B," MM<sub>B</sub>; (●) MM<sub>C</sub> through MM<sub>I</sub>; (□) serotonin; and (■) FRF<sub>A</sub> through FRF<sub>C</sub>. For details, see (29, 30). (B) Model. The relation between the Ca and K current values Ca and K and the contraction size S is assumed to have the form

$$S = \frac{S_{max}}{1 + \frac{k_S}{(Ca + a)\exp(-K/\kappa)}} \quad (1)$$

Although intracellular Ca<sup>2+</sup> concentration ([Ca<sup>2+</sup>]<sub>i</sub>)-contraction dynamics in the ARC muscle are likely to be more complex (31), this is a plausible, simple form, sufficient for our purposes here. It is motivated by the following considerations: (i) hyperbolic (for example, Michaelis-Menten) dependence of S on [Ca<sup>2+</sup>]<sub>i</sub>, (ii) [Ca<sup>2+</sup>]<sub>i</sub> proportional to Ca and its degree of activation, (iii) activation exponentially dependent on membrane voltage, and (iv) voltage proportional to K (19). The parameter a is required to satisfy S(Ca = 0, K = 0) = 100%; thus a = 100k<sub>S</sub>/(S<sub>max</sub> - 100). Fitting Eq. 1 to subsets of the data in (A) yields the particular surface plotted in (B), with S<sub>max</sub> = 400%, k<sub>S</sub> = 8%, κ = 9% (32). The SCP and MM dose-response trajectories on the surface (10<sup>-10</sup> to 10<sup>-4</sup> M, from left to right) were calculated by applying Eq. 1 to the Ca and K dose-response curves in Fig. 3, A and B.

Figure 3 shows dose-response relations for the Ca current, K current, and relaxation rate effects of the SCPs and MMs. All are fit with the same basic function

$$X_{modulator} = \frac{X_{max, modulator}}{1 + \left(\frac{K_x}{[modulator]}\right)^{h_x}} \quad (2)$$

where X is Ca, K, or R and the modulator is SCP or MM. To simplify subsequent combination of SCP and MM effects, where SCPs and MMs are known to act indistinguishably, data have been pooled or the fit constrained to yield identical parameter values. Means ± SEM are shown throughout. Regarding normalization of the data, see (30). (A) Ca current. Data from dose-response plots in (15, 18) for MM<sub>A</sub> through MM<sub>I</sub> (n = 3; n = 29 for 10<sup>-5</sup> M) and SCP<sub>B</sub> (n = 3). Best fit yields (for both SCP and MM) Ca<sub>max</sub> = 80%, k<sub>Ca</sub> = 4.3 × 10<sup>-8</sup> M, h<sub>Ca</sub> = 0.75. (B) K current. Data from dose-response plots in (15, 19) for MM<sub>A</sub> (n = 6) and SCP<sub>A</sub> and SCP<sub>B</sub> (n = 7 to 8). Best fit yields k<sub>K</sub> = 1.8 × 10<sup>-7</sup> M, h<sub>K</sub> = 0.85 (for both SCP and MM), K<sub>max,MM</sub> = 100% (by definition), K<sub>max,SCP</sub> = 27%. (C) Relaxation rate (R). Data from experiments done as in Fig. 1B, with SCP<sub>B</sub> (n = 8 to 11), MM<sub>A</sub> (n = 3 to 4), MM<sub>B</sub> (n = 4), and SCP<sub>B</sub> plus MM<sub>B</sub> (10<sup>-5</sup> M each, n = 4). MM<sub>B</sub> was used to supplement the MM<sub>A</sub> data particularly above 10<sup>-7</sup> M where MM<sub>A</sub> completely abolishes contractions; MM<sub>B</sub> activates K current and depresses contractions much less than MM<sub>A</sub> but has the same effect on relaxation rate [(15, 19) and this data]. Best fit yields (for both SCP and MM) R<sub>max</sub> = 100% (by definition), k<sub>R</sub> = 1.7 × 10<sup>-8</sup> M, h<sub>R</sub> = 0.7.

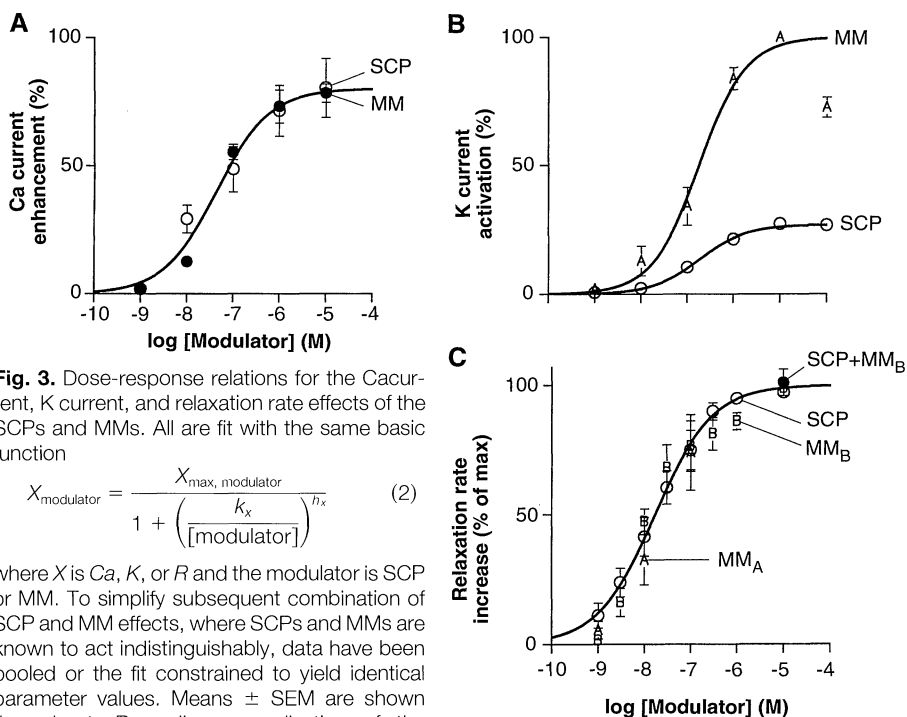


**Fig. 3.** Dose-response relations for the Ca current, K current, and relaxation rate effects of the SCPs and MMs. All are fit with the same basic function

To understand the interaction of the various elements, we first construct a quantitative model of how the modulation of the Ca and K currents affects contraction size. Then, knowing how the actions of SCPs and MMs combine at the level of the currents, we can predict how the combinations will change contraction size. We make similar predictions for the relaxation rate. We then test these predictions experimentally. Finally, we consider the contraction size and relaxation rate effects together.

In Fig. 2A we have plotted all available measurements of changes in contraction size with various modulator concentrations (from experiments like those in Fig. 1B) against the known Ca and K current effects of those concentrations. We have included not just SCPs and MMs but also other modulators that give yet other ratios of the effects on the Ca and K currents, to allow better definition of the surface relating modulation of the two currents to contraction size (17). The best surface (Fig. 2B) is a simple form fitted to the data in Fig. 2A. Contractions grow, in a saturating manner, with increasing Ca current; they diminish and eventually disappear with increasing K current. The "SCP" and "MM" curves illustrate how the effects of SCPs and MMs traverse different regions of the surface.

Figure 3 shows dose-response relations for the individual SCP and MM effects on the Ca current, K current, and relaxation rate. The sole difference between the effects of SCP and MM is the larger amplitude of MM-activated K current. In all three cases, large SCP and MM effects occlude each other, but smaller effects simply add, without synergism or other higher order interaction (15, 18, 19) ("SCP + MM<sub>B</sub>" in Fig. 3C; Fig. 4). This allows us to formulate simple rules for calculating the magnitude of each effect when SCPs and MMs are applied in arbitrary combination (Eqs. 3 and 4).

Using these combination rules together with the equation relating the Ca and K currents to contraction size, in Fig. 4 we have plotted the predicted modulation of contraction size and relaxation rate by a range of SCP-MM combinations and then tested these SCP-MM combinations experimentally. Given the variability inherent in these experiments (25), the model predictions are borne out well; the only significant discrepancy may be that the peak of potentiated contraction size appears at slightly higher SCP concentrations than predicted. The general agreement implies adequacy of the two main assumptions of the model, that modulation of the Ca and K currents is sufficient to explain the modulation of contraction size and the absence of higher-order interaction between the ef-

fects of SCP and MM.

To consider the contraction-size and relaxation-rate effects together, in Fig. 5A we plot the modeled contraction size and relaxation rate surfaces in Fig. 4 against each other. The solid curves in the left panel emphasize how the plot is traversed as SCP concentration varies in the presence of fixed MM; in the right panel, vice versa. In Fig.

5B, we plot in the same way experimental data from Fig. 4, selected for clarity to show the most important trends. Figure 5C shows representative individual contractions.

Two main conclusions emerge. First, the model predicts that all ratios of contraction size and relaxation rate intermediate between those given by pure SCP and pure MM should be obtainable with the SCP-

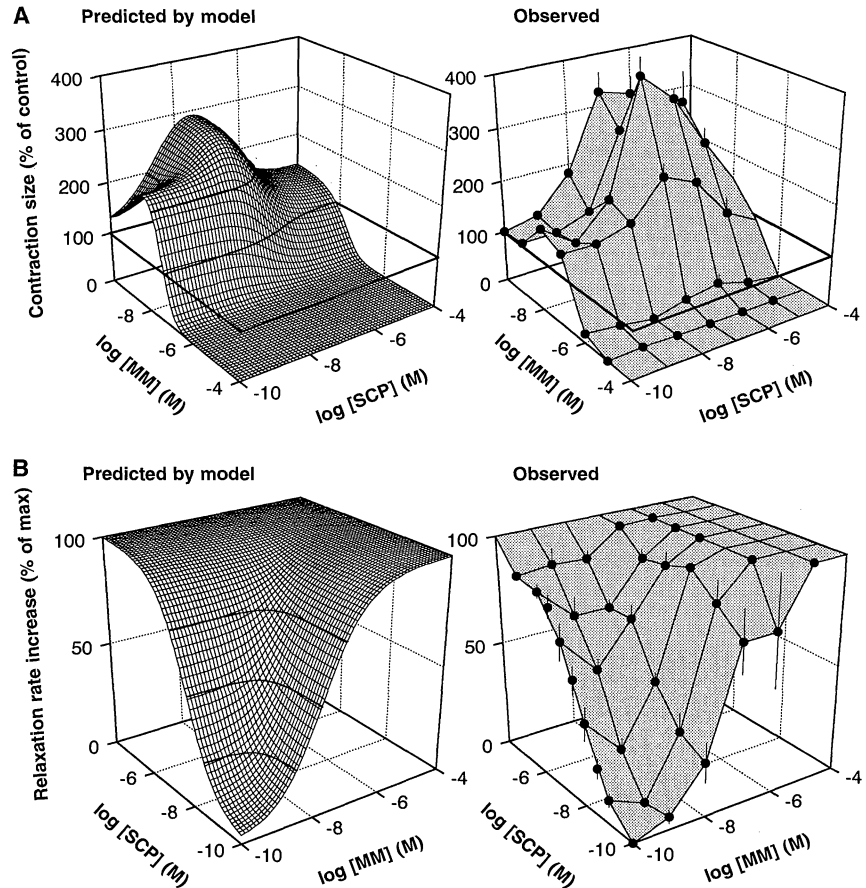


**Fig. 4.** Predicted and observed modulation of contraction size and relaxation rate by SCP-MM combinations. Combination rules for the three effects in Fig. 3 were devised as follows. Small Ca current, K current, and relaxation rate effects add, large effects occlude. On the Ca current and relaxation rate, SCP and MM act indistinguishably; only the total modulator concentration is important. The simplest combination rule is

$$X_{\text{combination}} = \frac{X_{\text{max}}}{1 + \left( \frac{k_x}{[\text{SCP}] + [\text{MM}]} \right)^{h_x}} \quad (3)$$

where  $X$  is  $Ca$  or  $R$ . On the K current, SCP and MM differ in  $K_{\text{max}}$ . A simple combination rule is

$$K_{\text{combination}} = K_{\text{SCP}} + \frac{K_{\text{max, MM}} - K_{\text{SCP}}}{1 + \left( \frac{k_K}{[\text{MM}]} \right)^{h_K}} \quad (4)$$

with  $K_{\text{SCP}}$  given by Eq. 2. **(A)** Contraction size. Combined Ca and K values were calculated with the use of Eqs. 3 and 4, and then contraction size was predicted by Eq. 1. The experiments were done as in Fig. 1B. Means  $\pm$  SEM are shown (average  $n = 7.8$ ). **(B)** Relaxation rate. Note that these plots are turned relative to those in (A). Predicted modulation was calculated with the use of Eq. 3. The observed values are from the experiments in (A), where any contraction remained (average  $n = 7.6$ ). The contraction size and relaxation rate measurements plotted for  $10^{-10}$  M SCP were in fact obtained with no SCP (that is, they are the dose-response relations for pure MM), and similarly with  $10^{-10}$  M MM. Some of the contraction size measurements in the peak region as well as some relaxation rate measurements are significantly different from the predicted values [ $t$  test,  $P < 0.05$  (25)].

MM combinations (Fig. 5A). Indeed, this is seen experimentally. Within certain limits, it appears that any effect on contraction size can be combined with any effect on relaxation rate (Fig. 5C), now making possible,

for example, the contractions unchanged in size but with greatly accelerated relaxation rate (extreme right of figure).

Functionally, the independent variability of the two parameters (or of more

biomechanical parameters that they reflect) most likely provides the flexibility required to integrate the contractions of this muscle with those of other muscles under different behavioral circumstances (16, 26). In different behaviors, B15 and B16 do indeed fire differentially, exposing the muscle to different, and apparently appropriate, SCP-MM combinations. For example, abbreviated movements that reject unsuitable food, in which a light, brief closure of the radula is needed, involve only B16, whereas full biting and swallowing movements, requiring strong closure to break off and pull in the food, also involve B15 (5). However, whether the contractions are large or small, in order to allow efficient alternation of the contractions of the ARC and its antagonist muscles, the relaxation rate must increase as the rate of feeding (which is governed by a central pattern generator) accelerates with food-induced arousal (27).

The second conclusion that emerges from Fig. 5 is perhaps more unexpected. When both SCP and MM are present at physiological concentrations around  $10^{-8}$  or  $10^{-7}$  M (28) (the general area circled in Fig. 5A), their effects become polarized, more sharply different than those of pure SCP and MM. The model predicts that SCP in the presence of a small amount of MM becomes a virtually pure modulator of relaxation rate (in Fig. 5A, left, the SCP dose-response curves are practically horizontal in the physiological concentration range), and MM in the presence of a small amount of SCP becomes a virtually pure modulator of contraction size (in Fig. 5A, right, the MM dose-response curves are practically vertical). In effect, the divergent and convergent linkages in the system become completely disconnected. Experimentally, MM behaves as predicted: it becomes a purer depressor (Fig. 5B, right). SCP, however, becomes a purer potentiator (Fig. 5B, left). This discrepancy can be traced to the fact that peak potentiation occurs at slightly higher SCP concentrations than those predicted. Thus, where in the model the potentiating and depressing effects of SCP cancel to leave just the modulation of relaxation rate, in fact the potentiation still dominates and is now purer as MM has already modulated the relaxation rate to some degree. Evidently, any one of the three effects of SCP and MM can become emphasized, depending critically on the exact nonlinearities in the system. These will themselves change with the physiological and behavioral circumstances, most obviously those resulting in the release of yet other convergent modulators. However, the basic mechanisms involved are simple and general. It is therefore very likely that phe-

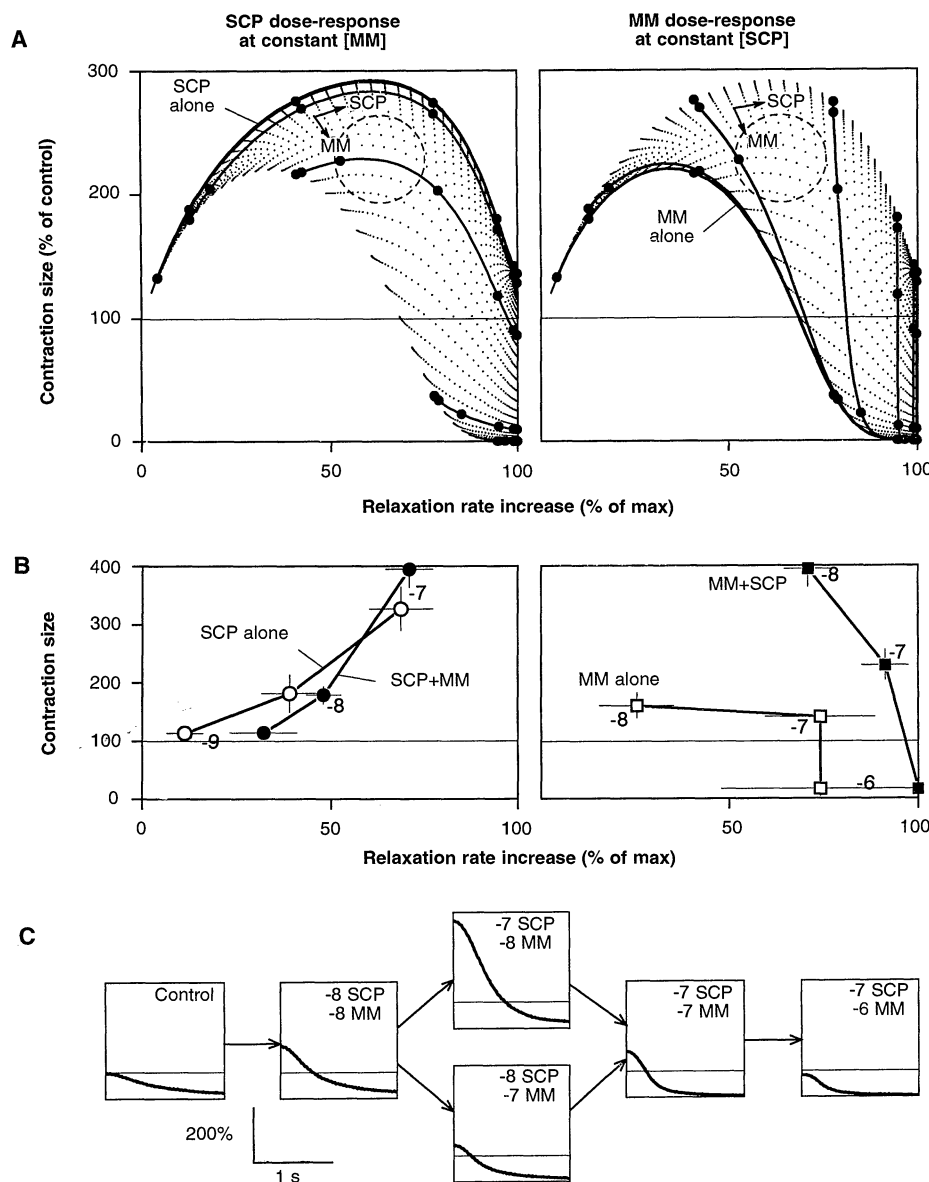


**Fig. 5.** The contraction size and relaxation rate effects considered together. **(A)** Predictions of model. The modeled contraction size and relaxation rate surfaces from Fig. 4 are plotted against each other. The grid of faint points reflects the grid of SCP and MM concentrations, each varying from  $10^{-10}$  to  $10^{-4}$  M in increments of 0.1 log unit (some regions of the space, especially at high MM concentration, are compressed and indistinguishable). The larger black dots indicate full order-of-magnitude increments. In the left panel, dots at the same MM concentration are connected; in the right panel, dots at the same SCP concentration are connected. The left panel thus shows SCP dose-response relations ( $10^{-10}$  to  $10^{-4}$  M from left to right of each curve) in the presence of  $10^{-10}$ ,  $10^{-9}$ , ...,  $10^{-4}$  M MM (top to bottom curves;  $>10^{-7}$  M compressed in bottom right corner); the right panel shows MM dose-response relations ( $10^{-10}$  to  $10^{-4}$  M from top to bottom of each curve;  $>10^{-7}$  M compressed) in the presence of  $10^{-10}$ ,  $10^{-9}$ , ...,  $10^{-4}$  M SCP (left to right curves). Dose-response relations for pure SCP and MM are also indicated. **(B)** Selected experimental observations from Fig. 4, plotted as in (A). Means  $\pm$  SEM are shown. (Left) SCP dose-response relation between  $10^{-9}$  and  $10^{-7}$  M, alone and in the presence of  $10^{-8}$  M MM; (right) MM dose-response relation between  $10^{-8}$  and  $10^{-6}$  M, alone and in the presence of  $10^{-7}$  M SCP. **(C)** Relaxation phases of individual contractions, selected from the experiments in Fig. 4, illustrating the wide range of contraction size:relaxation rate ratios obtained with SCP-MM combinations. “-8,” “-7,” and “-6” indicate  $10^{-8}$ ,  $10^{-7}$ , and  $10^{-6}$  M, respectively.

nomena of this kind are to be found in many, if not most, physiological signaling systems.

## REFERENCES AND NOTES

1. F. E. Bloom, *FASEB J.* **2**, 32 (1988); R. A. Nicoll, *Science* **241**, 545 (1988); I. Kupfermann, *Physiol. Rev.* **71**, 683 (1991).
2. B. Hille, *Neuron* **9**, 187 (1992).
3. *Trends Biochem. Sci.* **17** (no. 10) (1992); H. R. Bourne and R. Nicoll, *Cell* **72/Neuron** **10** (suppl.), 65 (1993); F. L. Bygrave and H. R. Roberts, *FASEB J.* **9**, 1297 (1995); R. lyengar, *Science* **271**, 461 (1996).
4. J. L. Cohen, K. R. Weiss, I. Kupfermann, *J. Neurophysiol.* **41**, 157 (1978).
5. E. C. Cropper, I. Kupfermann, K. R. Weiss, *Brain Res.* **522**, 176 (1990); P. J. Church and P. E. Lloyd, *J. Neurophysiol.* **72**, 1794 (1994).
6. K. R. Weiss, J. L. Cohen, I. Kupfermann, *J. Neurophysiol.* **41**, 181 (1978).
7. E. C. Cropper *et al.*, *Proc. Natl. Acad. Sci. U.S.A.* **85**, 6177 (1988).
8. E. C. Cropper *et al.*, *J. Neurophysiol.* **72**, 2181 (1994).
9. P. E. Lloyd, I. Kupfermann, K. R. Weiss, *Proc. Natl. Acad. Sci. U.S.A.* **81**, 2934 (1984).
10. E. C. Cropper *et al.*, *ibid.* **84**, 3486 (1987).
11. E. C. Cropper *et al.*, *ibid.*, p. 5483; E. C. Cropper *et al.*, *Peptides* **12**, 683 (1991).
12. M. D. Whim and P. E. Lloyd, *J. Neurosci.* **10**, 3313 (1990).
13. ———, *Proc. Natl. Acad. Sci. U.S.A.* **86**, 9034 (1989).
14. E. C. Cropper *et al.*, *ibid.* **87**, 933 (1990).
15. V. Brezina *et al.*, *J. Neurophysiol.* **74**, 54 (1995).
16. K. R. Weiss *et al.*, *J. Physiol. (Paris)* **87**, 141 (1993).
17. For most modulators in the ARC-muscle system, the available evidence suggests that the effects on contractions can be fully explained by direct action on the muscle fibers, through the pathways in Fig. 1A only [(15, 18, 19); V. Brezina and K. R. Weiss, *Soc. Neurosci. Abstr.* **19**, 1262 (1993)]. This holds for the SCPs and MMs, as well as the serotonin and FMRF amide-related peptide (FRF) effects in Fig. 2A. Indirect modulation of contractions through changes in transmitter release from the motor neurons—for example, by the buccalins (7, 16)—is not considered here.
18. V. Brezina, C. G. Evans, K. R. Weiss, *J. Neurosci.* **14**, 4393 (1994).
19. ———, *ibid.*, p. 4412.
20. W. C. Probst *et al.*, *Proc. Natl. Acad. Sci. U.S.A.* **91**, 8487 (1994).
21. K. R. Weiss *et al.*, *J. Neurophysiol.* **42**, 791 (1979).
22. S. L. Hooper *et al.*, *Brain Res.* **657**, 337 (1994); S. L. Hooper *et al.*, *Neurosci. Lett.* **179**, 167 (1994).
23. It is likely that B16 co-releases at least nine MMs, MM<sub>A</sub> through MM<sub>I</sub> (15), which act identically in most respects but differ in their ability to activate the K current (15, 19). MM<sub>B</sub> and MM<sub>C</sub> are not much more effective than the SCPs. However, the other seven MMs activate large K currents, and the most effective of all, MM<sub>A</sub>, is overrepresented in the likely released mixture. Thus, the overall effect of MM release from B16 is activation of a large K current as with MM<sub>A</sub> alone (15). In our experiments here, we therefore apply just MM<sub>A</sub> (except in Fig. 3C). Similarly, B15 co-releases SCP<sub>A</sub> and SCP<sub>B</sub>, which act identically in all respects [(10); P. E. Lloyd, *Trends Neurosci.* **9**, 428 (1986)]; we apply just SCP<sub>B</sub>.
24. Strictly, the convergence on cAMP is not equal: SCPs can elevate cAMP much higher than MMs can (9, 18, 22). However, what matters for our purposes here is that the downstream effects of the SCPs and MMs on the Ca current (18) (Fig. 3A) and the relaxation rate (Fig. 3C) are equal, probably because only relatively small increases in cAMP are important: for example, they suffice to enhance the Ca current maximally (18).
25. In addition to somewhat different experimental protocols (29), major variability in this work is due to differences between animals and especially between batches of animals used in different seasons or years. Differences between batches can be much larger than those within each batch. This can be a serious problem in a study such as this that correlates a variety of data sets. As a result, for instance, we cannot be sure that the deviations of the experimental data in Fig. 4 from the model predictions are not simply the result of somewhat different responses of the animals used in the experiments and those used to obtain the data on which the model was based. This provides one justification for keeping the modeling simple and focused only on major features.
26. I. Kupfermann *et al.*, in *Neurons, Networks, and Motor Behavior*, P. S. G. Stein *et al.*, Eds. (MIT Press, Cambridge, MA, in press).
27. A. J. Susswein, K. R. Weiss, I. Kupfermann, *J. Comp. Physiol. A* **123**, 31 (1978).
28. We obtained these estimates by comparing the effects of B15 and B16 stimulation at physiological frequencies and the effects of known concentrations of exogenous SCP and MM [on, for example, cAMP and active protein kinase A (PKA) concentrations in the muscle (22)]. With more intense stimulation, the concentration of SCP released from B15 may reach as high as 10<sup>-5</sup> M (13).
29. The contraction measurements are from figures in (6–9, 11, 15), older unpublished experiments, and experiments done specifically for this report (for example, Fig. 1B): SCP<sub>A</sub> and SCP<sub>B</sub>, 117 measurements from 40 preparations; MM<sub>A</sub>, 20 from 12; MM<sub>B</sub>, 47 from 10; MM<sub>C</sub>, through MM<sub>I</sub>, 66 from 28; serotonin, 2 from 2; and FRF<sub>A</sub> through FRF<sub>C</sub>, 15 from 6. The older experiments were all done basically as in Fig. 1B but with occasional variations [for example, stimulation of B15 rather than B16, shorter interburst intervals (but not less than 10 s), or shorter modulator exposure before measurement (but not less than 2.5 min)], which may account for some of the variability. The Ca and K current values are mean values ( $n = 3$  to 7) pooled from dose-response plots in (8, 15, 18, 19); where necessary, linear interpolation was used, along with the fact that SCP<sub>A</sub> and SCP<sub>B</sub> act identically (23), as do FRF<sub>A</sub> through FRF<sub>C</sub> (8) and, on the Ca current, MM<sub>A</sub> through MM<sub>I</sub> (15, 18) (Fig. 3, A and B, shows a subset of the same data). The FRFs are assumed not to modulate the Ca current (8). For normalization of the data, see (30).
30. Contraction size is always expressed as a percentage of control size (control = 100%, no contraction = 0%), Ca current enhancement is expressed as the percentage increase over control current amplitude (control = 0%), and K current activation is expressed as a percentage of the current activated by saturating MM<sub>A</sub>, which is the largest and occludes all others (8, 15, 19) (no current = 0%, saturating MM<sub>A</sub> = 100%) (desensitization of the K current response is ignored). Relaxation rate is expressed as a percentage of the range within each experiment (control = 0%, fastest rate induced by high SCP or MM = 100%). In Fig. 3C, SCP and MM were tested in separate experiments; however, the following information shows that 100% represents essentially the same absolute maximal effect for both. In four of the experiments with SCP<sub>B</sub> and four matched experiments with MM<sub>B</sub>, SCP<sub>B</sub> increased the relaxation rate from 0.87 ± 0.05 s<sup>-1</sup> (= 0%) to 3.99 ± 0.90 s<sup>-1</sup> (= 100%), and MM<sub>B</sub> increased it from 1.06 ± 0.09 to 4.01 ± 0.61 s<sup>-1</sup> (mean ± SEM). Moreover, maximal SCP and MM effects were mutually occlusive ("SCP + MM<sub>B</sub>").
31. V. Brezina and K. R. Weiss, *J. Neurophysiol.* **73**, 993 (1995); *Biophys. J.* **68**, A277 (1995).
32. Quantification of the vertical scatter of the points in Fig. 2A from the surface in Fig. 2B. The mean deviation (experimental – model) and the standard deviation, respectively (in percent): all points, 8.3 and 6.4; SCP<sub>A</sub> and SCP<sub>B</sub>, –13.5 and 12.0; MM<sub>A</sub>, 66.0 and 21.0; MM<sub>B</sub>, 33.3 and 15.8; MM<sub>C</sub>, through MM<sub>I</sub>, 7.8 and 5.0; and FRF<sub>A</sub> through FRF<sub>C</sub>, 8.2 and 6.1 (too few points were available for serotonin). Thus, the points for each modulator lie reasonably evenly above and below and not too far from the surface, except for MM<sub>A</sub> and MM<sub>B</sub>, which lie somewhat more above the surface.
33. We thank E. C. Cropper and B. Bank for the unpublished data included in Fig. 2A, and E. C. Cropper, M. L. Scott, C. Exleben, and I. Kupfermann for comments on the manuscript. This work was funded by NIH grants MH36730, GM320099 (K.R.W.), and K21 MH00987 (V.B.) and the Whitehall Foundation (V.B.).

5 April 1996; accepted 30 May 1996

## Organization of Diphtheria Toxin T Domain in Bilayers: A Site-Directed Spin Labeling Study

Kyoung Joon Oh, Hangjun Zhan,\* Can Cui, Kálmán Hideg, R. John Collier,† Wayne L. Hubbell‡

The diphtheria toxin transmembrane (T) domain was spin-labeled at consecutive residues in a helical segment, TH9. After binding of the T domain to membranes at low pH, the nitroxide side chains generated by spin labeling were measured with respect to their frequency of collision with polar and nonpolar reagents. The data showed that the helical structure of TH9 in solution is conserved, with one face exposed to water and the other to the hydrophobic interior of the bilayer. Measurement of the depth of the nitroxide side chains from the membrane surfaces revealed an incremental change of about 5 angstroms per turn, which is consistent with a transmembrane orientation of an  $\alpha$  helix. These results indicate that the helix forms the lining of a transmembrane water-filled channel.

Diphtheria toxin (DT) (1) belongs to a large class of toxic proteins that act by enzymatically modifying cytosolic substrates within eukaryotic cells (2). The process by which the catalytic moiety is transferred across a membrane lipid bilayer into the cytosol is not understood for any such toxin. For DT, translocation occurs only after the toxin has bound to its receptor at the cell surface and has been delivered by receptor-

mediated endocytosis to the endosomal compartment (3). Under the influence of the low pH within that compartment, the toxin undergoes a conformational rearrangement that causes its T domain to insert into the endosomal membrane (4). This insertion event is known to induce the toxin's catalytic domain to cross the membrane to the cytosolic compartment (5), where it catalyzes the adenosine diphos-